The EMBO Journal Vol. 22 No. 22 pp. 6004–6015, 2003

Bicaudal D induces selective dynein-mediated microtubule minus end-directed transport

Casper C.Hoogenraad[1], Phebe Wulf[1], Natalia Schiefermeier[2], Tatiana Stepanova[3], Niels Galjart[3], J.Victor Small[2], Frank Grosveld[3], Chris I.de Zeeuw[1] and Anna Akhmanova[3,4]

MGC Departments of [1]Neuroscience and [3]Cell Biology and Genetics, Erasmus University, PO Box 1738, 3000 DR Rotterdam, The Netherlands and [2]Institute of Molecular Biology, Austrian Academy of Sciences, Billrothsthstrasse 11, Salzburg 5020, Austria

[4]Corresponding author
e-mail: anna.akhmanova@chello.nl

Bicaudal D is an evolutionarily conserved protein, which is involved in dynein-mediated motility both in *Drosophila* and in mammals. Here we report that the N–terminal portion of human Bicaudal D2 (BICD2) is capable of inducing microtubule minus end-directed movement independently of the molecular context. This characteristic offers a new tool to exploit the relocalization of different cellular components by using appropriate targeting motifs. Here, we use the BICD2 N–terminal domain as a chimera with mitochondria and peroxisome-anchoring sequences to demonstrate the rapid dynein-mediated transport of selected organelles. Surprisingly, unlike other cytoplasmic dynein-mediated processes, this transport shows very low sensitivity to overexpression of the dynactin subunit dynamitin. The dynein-recruiting activity of the BICD2 N–terminal domain is reduced within the full-length molecule, indicating that the C–terminal part of the protein might regulate the interaction between BICD2 and the motor complex. Our findings provide a novel model system for dissection of the molecular mechanism of dynein motility.
Keywords: cytoplasmic dynein/dynactin/kinesin/mitochondria/peroxisomes

Introduction

Cytoplasmic dynein is a large multiprotein complex, which is responsible for transporting various cargos to the minus ends of microtubules (for review, see Hirokawa *et al*., 1998; Karki and Holzbaur, 1999). The molecular mechanism of dynein translocation along microtubules and its recognition of different cargos is not yet fully elucidated. It is established that another multiprotein complex, dynactin, is necessary for most, if not all types of dynein transport (Schroer, 1996; Allan, 2000). Dynactin has been shown to improve dynein processivity and to mediate its interaction with different cellular structures (Echeverri *et al*., 1996; King and Schroer, 2000; Muresan *et al*., 2001; Helfand *et al*., 2002). In addition, a number of cargos have been shown to bind to dynein directly via one of its subunits (Purohit *et al*., 1999; Tai *et al*., 1999; Schnorrer *et al*., 2000; Ligon *et al*., 2001).

Bicaudal D protein was initially identified as a component of dynein pathway by genetic analysis in *Drosophila* (Suter *et al*., 1989; Wharton and Struhl, 1989; Swan *et al*., 1999) and recent studies demonstrated its involvement in dynein-mediated mRNA transport (Bullock and Ish-Horowicz, 2001). However, the exact role of this protein at the molecular level remained unclear. In mammals, two homologues of Bicaudal D, BICD1 and BICD2, are present (Baens and Marynen, 1997; Hoogenraad *et al*., 2001). Studies in cultured mammalian cells have shown that BICD proteins bind to the small GTPase Rab6, as well as to dynein and dynactin complexes, and therefore participate in recruitment of dynein motor to Rab6-positive membranes of the Golgi apparatus and cytoplasmic vesicles (Hoogenraad *et al*., 2001; Matanis *et al*., 2002; Short *et al*., 2002). However, in addition to BICD proteins, Rab6 GTPase can also interact directly with the $p150^{Glued}$ component of the dynactin complex (Short *et al*., 2002). This raises the possibility that BICD acts as an accessory factor for the dynein motor, but is not sufficient by itself to recruit it to organelles.

BICD proteins consist of several coiled-coil domains, and our previous studies have demonstrated that while the C–terminal domain is responsible for interaction with membranes via Rab6, the N–terminal domain binds to cytoplasmic dynein (Hoogenraad *et al*., 2001; Matanis *et al*., 2002). In addition, we observed that the N- and C–terminal domains of BICD can interact with each other. Based on these findings, we proposed that when BICD binds to the cargo (cytoplasmic vesicle) via its C–terminal domain, the N–terminal domain of BICD2 becomes available for interaction with dynein motor, which, in its turn, would transport the vesicle. If this model is correct, tethering of the BICD N–terminus to membranous organelles, which are normally devoid of BICD (such as mitochondria or peroxisomes), should be sufficient to induce their transport by cytoplasmic dynein. In this study, we test this idea and show that the N–terminal part of BICD2 protein is indeed a potent recruitment factor for dynein, and that it can act in different molecular contexts.

Results

Targeting of BICD2 N–terminus to mitochondria and peroxisomes causes their relocalization to the microtubule organizing centre

To test the recruiting capacity of the BICD protein for cytoplasmic dynein, we decided to use the membrane-targeting sequence (MTS) of the ActA protein of *Listeria monocytogenes* (Pistor *et al*., 1994). This domain, constituting the last 26 amino acids of the ActA protein was

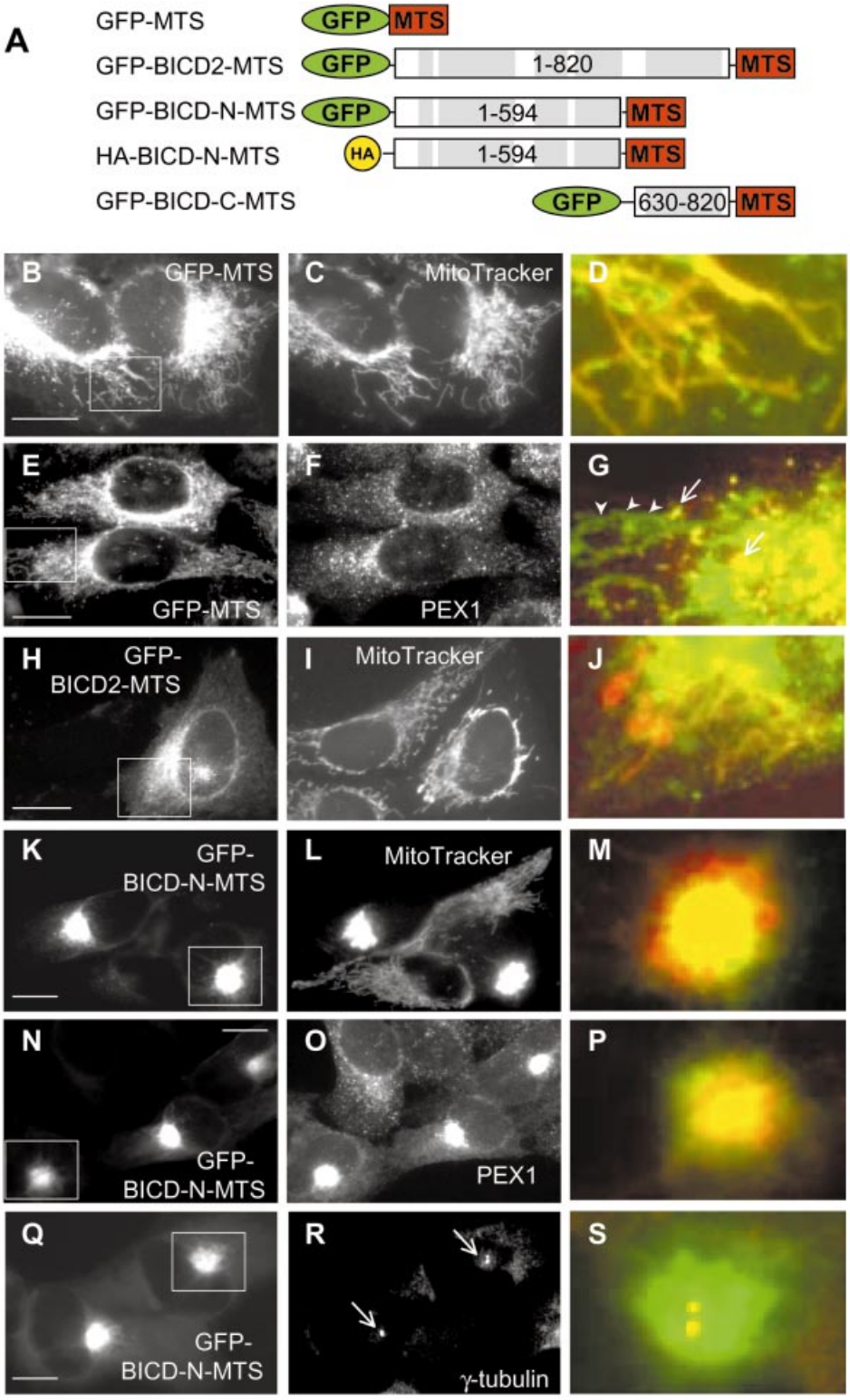

Fig. 1. Targeting of BICD2 N–terminus to mitochondria and peroxisomes induces their relocalization. (**A**) Schematic representation of the fusion constructs of BICD2 or its domains to membrane targeting sequence (MTS) of ActA protein of *Listeria monocytogenes*. Coiled-coil regions of BICD2 are indicated with gray boxes. (B–S) HeLa cells were transfected with GFP-fusion constructs and stained for different cytoplasmic organelles. GFP signals are shown in the left panel, stained organelles in the middle panels, and an overlay of the portion of the figure, indicated by a white rectangle, (with GFP signal in green, organelles in red), in the right panels. (**B–D**) Cells were transfected with GFP-MTS and stained for mitochondria with MitoTracker Red CMXRos. (**E–G**) Cells were transfected with GFP-MTS and stained for a peroxisomal marker PEX1 [in (G) peroxisomes are indicated by arrows, and mitochondria by arrowheads]. (**H–J**) Cells were transfected with GFP-BICD2-MTS and stained for mitochondria. (**K–S**) Cells were transfected with GFP-BICD-N-MTS and stained for mitochondria (L), peroxisomes (O), and a centrosomal marker γ-tubulin (R). MTOCs are indicated by arrows in (R). Bar, 10 μm.

successfully employed to target heterologous proteins to the cytoplasmic side of the outer mitochondrial membrane (Bubeck *et al*., 1997; Bear *et al*., 2000). As a control, we have fused this domain to GFP (GFP–MTS) (Figure 1A) and transfected it into HeLa cells. As expected, the fusion protein was targeted to mitochondria (Figure 1B–D), and, in addition, to smaller vesicle-like structures which were identified as peroxisomes by staining them for peroxisomal protein PEX1 (Figure 1E–G; data not shown). Peroxisomal localization of the membrane-anchoring domain of ActA was not described before, but may either reflect cell type-specific differences or the properties of this particular protein fusion.

When the full-length BICD2, fused to the MTS (Figure 1A), was expressed in HeLa cells, it was localized to both mitochondria (Figure 1H–J) and peroxisomes (Figure 7D–F). It caused their shift from normal cytoplasmic distribution to the perinuclear area (where the minus ends of microtubules are tethered), as would be expected if these organelles were transported by cytoplasmic dynein. The extent of relocalization was dependent on the concentration of the fusion protein; it varied from almost no effect at low expression level to formation of Golgi-like perinuclear aggregate of mitochondria and peroxisomes at high expression levels (see Materials and methods for the quantification of expression levels).

The C–terminal coiled-coil domain of BICD2, when fused to MTS (Figure 1A), did not localize to Rab6-positive vesicles, indicating that MTS interfered with normal membrane targeting of BICD. It preferentially localized to peroxisomes and more weakly to mitochondria, but had no effect on their subcellular distribution (data not shown). This result is in line with our previous observation that BICD C–terminus is not able by itself to recruit dynein and dynactin to Rab6-bound membranes (Matanis *et al*., 2002).

However, when the N–terminal portion of BICD2 was fused to MTS (GFP–BICD-N–MTS, Figure 1A) and transfected into HeLa cells, it caused dramatic relocalization of both mitochondria (Figure 1K–M) and peroxisomes (Figure 1N–P). Instead of being distributed throughout the cytoplasm, these organelles were accumulated in a tight perinuclear cluster, and mitochondria often lost their normal shape, appearing as rounded structures with a halo of GFP–BICD-N–MTS fusion protein at their surface (Figure 1M). This perinuclear cluster was always formed around the microtubule-organizing centre (MTOC) (as shown in Figure 1Q–S, where the MTOC is identified by staining for γ-tubulin). This effect was observed in all transfected cells, even at low levels of expression of the fusion protein. The same effect was observed in other types of cultured cells, including COS-1, Rat2 and CAR fish fibroblasts. The mitochondrial clusters, induced by GFP–BICD-N–MTS, appeared much more dense than those induced when the full-length BICD2 protein was fused to MTS. This result suggests that mitochondria and peroxisomes are actively transported to the MTOC in GFP–BICD-N–MTS-transfected cells.

The localization of the Golgi apparatus, endosomes and endoplasmic reticulum appeared normal in cells expressing moderate levels of GFP–BICD-N–MTS (See Supplementary figure 1, available at *The EMBO Journal* Online; and data not shown). However the Golgi stacks appeared to be somewhat displaced from their normal position around the MTOC, probably due to the sterical hindrance caused by the clustered mitochondria and peroxisomes (Supplementary figure 1B and C). In cells expressing very high levels of GFP–BICD-N–MTS, mitochondria and peroxisomes were still tightly clustered, while the Golgi apparatus was dispersed and perinuclear concentration of recycling endosomes was no longer visible. This indicates that at moderate expression levels, GFP–BICD-N–MTS did not interfere with the normal function of microtubule motors, while at high expression levels dynein transport of other cytoplasmic organelles was inhibited, probably because of its relocalization to the mitochondrial aggregate (see below).

To achieve a more specific targeting of the N–terminal portion of BICD2, we have fused it to the C–terminus of PEX3, an integral peroxisomal protein (Figure 2A). A

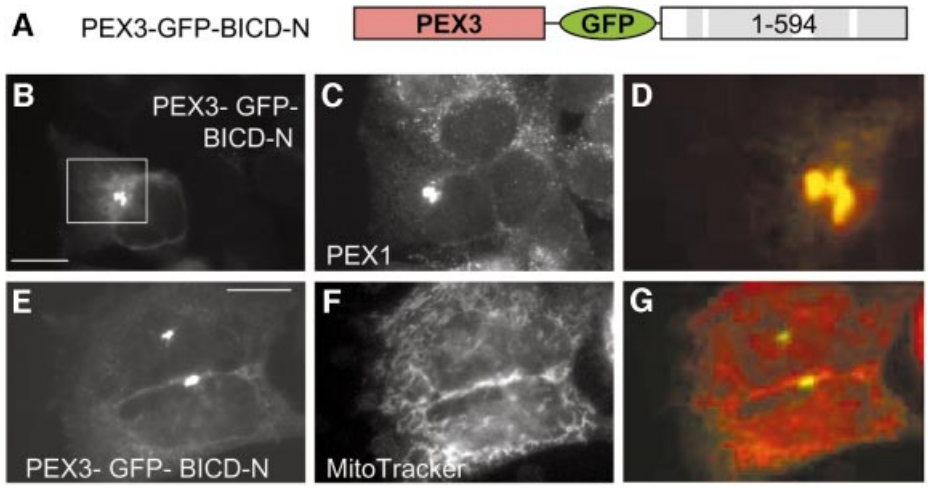

Fig. 2. BICD2 N–terminus, fused to PEX3, relocalizes peroxisomes, but not mitochondria. (**A**) Schematic representation of the PEX3–GFP–BICD-N fusion construct. (**B**–**G**) HeLa cells were transfected with PEX3–GFP–BICD-N fusion construct and stained for peroxisomes (C) or mitochondria (F). GFP signals are shown in the left panel, stained organelles in the middle panels, and an overlay (with GFP signal in green, organelles in red) in the right panel. Bar, 10 μm.

control PEX3–GFP fusion was targeted to peroxisomes, but not to mitochondria or other membrane organelles (Soukupova *et al*., 1999; and data not shown). Expression of PEX3–GFP–BICD-N fusion caused redistribution of all peroxisomes into a perinuclear position (Figure 2B–D). Peroxisomal clusters, formed in such cells, appeared much smaller than those observed with GFP–BICD-N–MTS (Figure 2N–P), because they only contained peroxisomes, while mitochondria were distributed normally (Figure 2E–G).

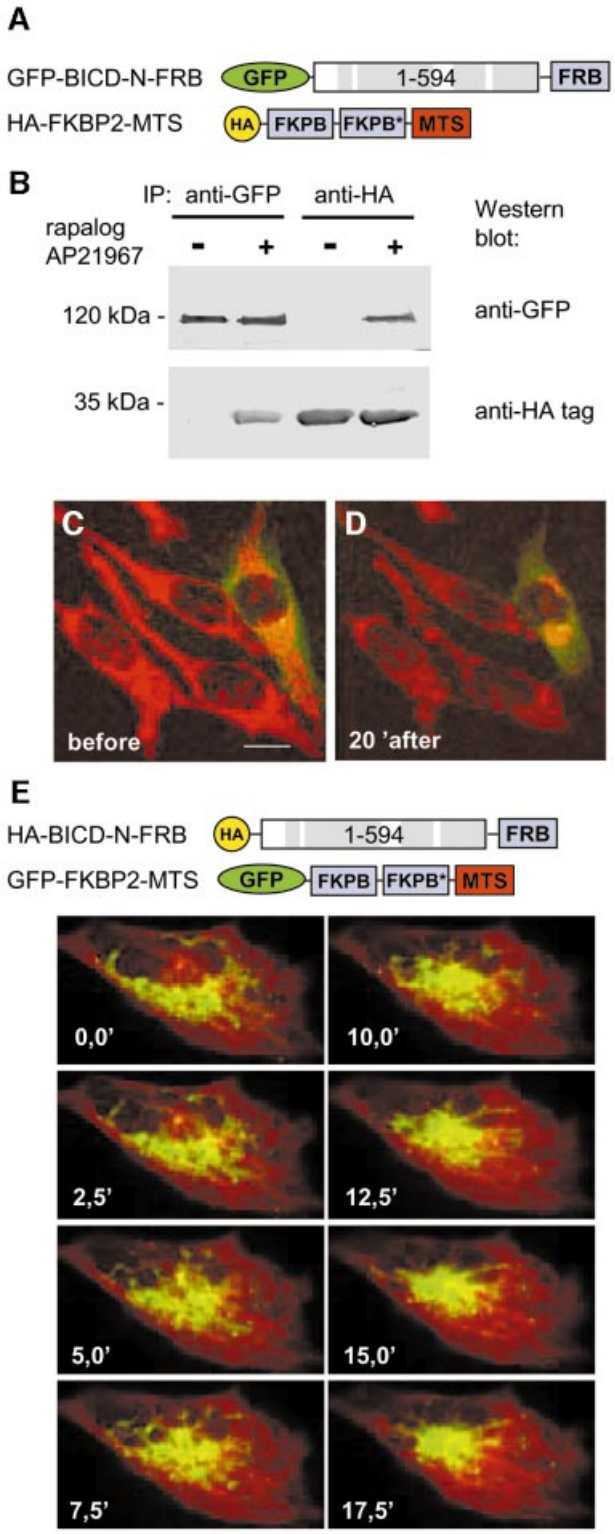

This observation shows that BICD-N can act in different molecular contexts.

We attempted to induce microtubule minus end-directed transport of mitochondria or peroxisomes by linking the MTS directly to one of the dynein subunits. We have fused the MTS to the C–termini of the dynein light intermediate chain 2 (LIC2) and dynein intermediate chain 2 (IC2) (Supplementary figure 2A). Both fusions were targeted to the organelles without causing their redistribution to the MTOC (Supplementary figure 2B–G). Naturally, it is quite possible that fusion to the MTS interfered with the incorporation of these subunits into the dynein complex. However, this experiment shows that targeting of the dynein motor activity to particular membranes in this fashion is not trivial and emphasizes an interesting and so far unique property of BICD N–terminus to cause such targeting.

Inducible tethering of BICD2 N–terminus to organelles causes their rapid microtubule minus end-directed movement

To analyze the kinetics of organelle relocalization, induced by tethering of the BICD N–terminus to their surface, we made use of the rapamycin-based regulated heterodimerization system (Rivera *et al*., 1996). This system utilizes the fact that FKBP12 and FRAP (mTOR) proteins bind to each other with high affinity in the presence of rapamycin. Two copies of the rapamycin-binding domain of the human FKBP12 protein (FKBP) were fused to the MTS and an HA-tag (Figure 3A). This construct was targeted to the mitochondria and peroxisomes, without altering their distribution (Supplementary figure 3A and B). A copy of the FRAP domain, which binds to the FKBP12–rapamycin complex (FRB), was added to the C–terminus of the GFP–BICD-N fusion (Figure 3A). We have used a modified version of the FRB domain, which can heterodimerize with FKBP in the presence of non-immunosuppressive rapamycin analogue AP21967. The advantage of this system is that binding between FRB and FKBP domains can be induced without stimulating endogenous FRAP (Pollock *et al*., 2000). When the two fusion proteins were coexpressed in HeLa

Fig. 3. Inducible targeting of BICD N–terminus to mitochondria, using regulated heterodimerization system. (**A**) Schematic representation of the fusion constructs. In the HA–FKBP2–MTS fusion the two FKBP domains differ by a number of synonymous substitutions, which reduce the recombination potential between the two tandem repeats (indicated by an asterisk). (**B**) HeLa cells were cotransfected with the two constructs, shown in (A), and used for immunoprecipitation with anti-GFP or anti-HA antibodies, and the immunoprecipitates were analyzed by western blotting. Where indicated with '+', AP21967 (125 nM) was added to the cells 2 h before preparing the lysate. (**C** and **D**) HeLa cells, transfected with GFP-BICD-N-FRB and HA-FKBP2-MTS, were analyzed 1 day after transfection by confocal microscopy. Cells were stained for mitochondria with MitoTracker Red CMXRos for 30 min, washed and maintained in normal culture medium at 37°C. Cells before (C) and 20 min after the addition of 125 nM AP21967 (D) are shown. The transfected cell can be distinguished by green cytoplasmic signal, corresponding to the GFP–BICD-N–FRB fusion protein. (**E**) CAR fish fibroblasts were transfected with HA-BICD-N-FRB and GFP-FKBP2-MTS. Forty-eight hours after transfection, cells were microinjected with Cy3–tubulin. Cells were treated with 250 nM AP21967 and images were taken at the indicated times after the dimerizer addition. Note that the MTOC is clearly visible as the point of microtubule convergence. Bar, 10 μm.

cells in the absence of the dimerizer AP21967, they did not bind to each other (Figure 3B). GFP–BICD-N–FRB protein showed predominantly diffuse cytoplasmic distribution (for details, see below), as was previously described for GFP–BICD-N, and mitochondria and peroxisomes were distributed throughout the cytoplasm, as in non-transfected cells (Supplementary figure 3C and D). The addition of the dimerizer AP21967 to the culture medium resulted in a rapid relocalization of mitochondria and peroxisomes to the perinuclear region. A large proportion (~75%) of transfected cells displayed a ring-like accumulation of mitochondria around the nucleus already after 5 min of drug treatment (Supplementary figure 3E and F), and 15–20 min after drug addition an aggregate of mitochondria around the MTOC was visible in most (~80%) transfected cells (Supplementary figure 3G–J). These observations were confirmed by following mitochondria in live cells using Mitotracker (Figure 3C and D; Supplementary movie 1).

To prove further that the mitochondrial cluster is not formed by random aggregation of mitochondria but by their directional movement to the MTOC, we have cotransfected CAR fish fibroblasts with GFP–FKBP2–MTS (which was targeted to mitochondria and peroxisomes, providing these organelles with a green fluorescent label) and HA–BICD-N–FRB (Figure 3E). To visualize the microtubules and the MTOC, the cells were microinjected with Cy3-labeled tubulin. Before the addition of the dimerizer, the GFP-labelled organelles displayed no directional motility (Supplementary movies 2A and 3A). However, immediately after the addition of the dimerizer, the GFP-labelled organelles started to converge to the MTOC, moving along the microtubule tracks (Supplementary movies 2B and 3B; Figure 3E) and

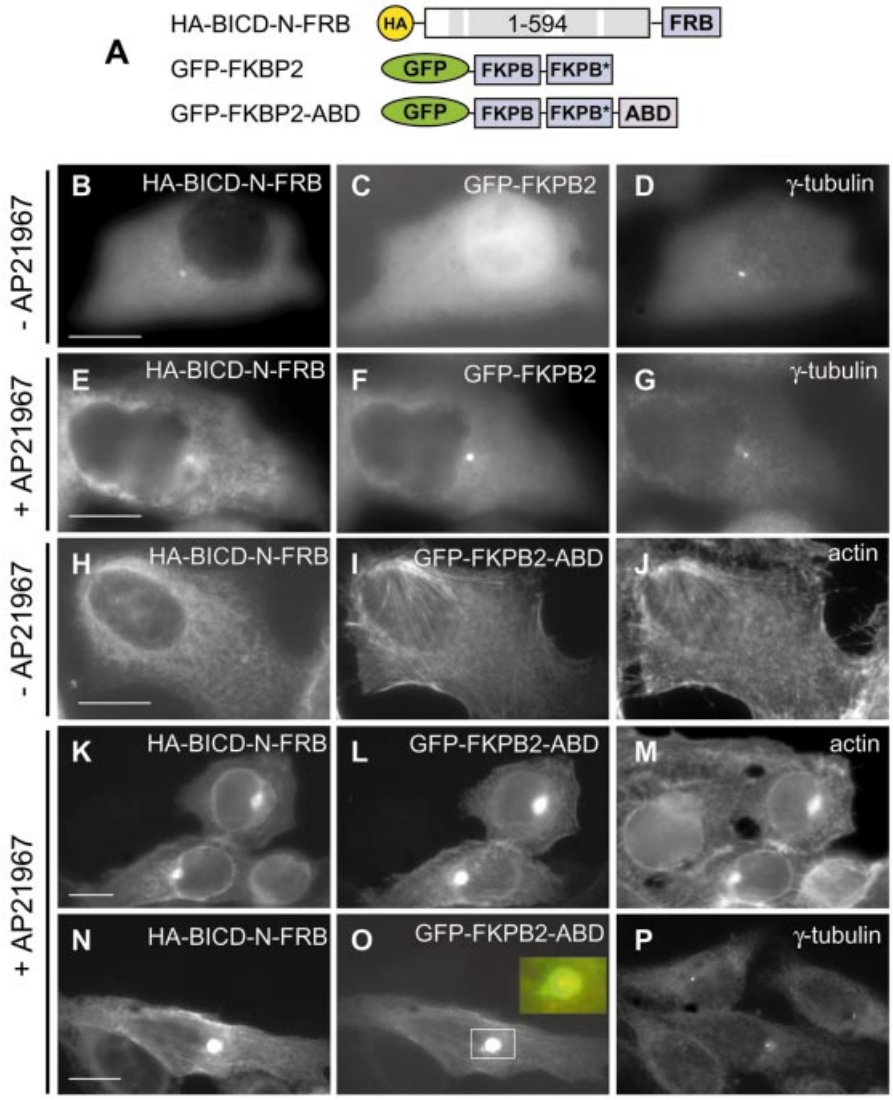

Fig. 4. BICD N–terminus relocalizes proteins to the MTOC. (**A**) Schematic representation of the constructs. (B–G) HeLa cells were transfected with HA-BICD-N-FRB (left panels) and GFP-FKBP2 (middle panels) and stained for γ-tubulin (right panels). Cells were either untreated with AP21967 (**B–D**), or treated with 125 nM AP21967 for 1 h (**E–G**). (**H–P**) HeLa cells were transfected with HA–BICD-N–FRB (left panels) and GFP–FKBP2–ABD (middle panels) and stained either for actin (J and M) or for γ-tubulin (P). The inset in (O) shows the enlarged portion of the GFP-containing aggregate (green), with the γ-tubulin-positive centrosome in the middle (red). Cells were either untreated with AP21967 (H–J), or treated with 125 nM AP21967 for 1 h (K–P). Bar, 10 μm.

forming a tight cluster, which colocalized with the MTOC, ~15 min after the dimerizer addition. Quick directional movement of mitochondria to the perinuclear area after induced recruitment of BICD N–terminal domain is most easily explained by activation of their transport by cytoplasmic dynein.

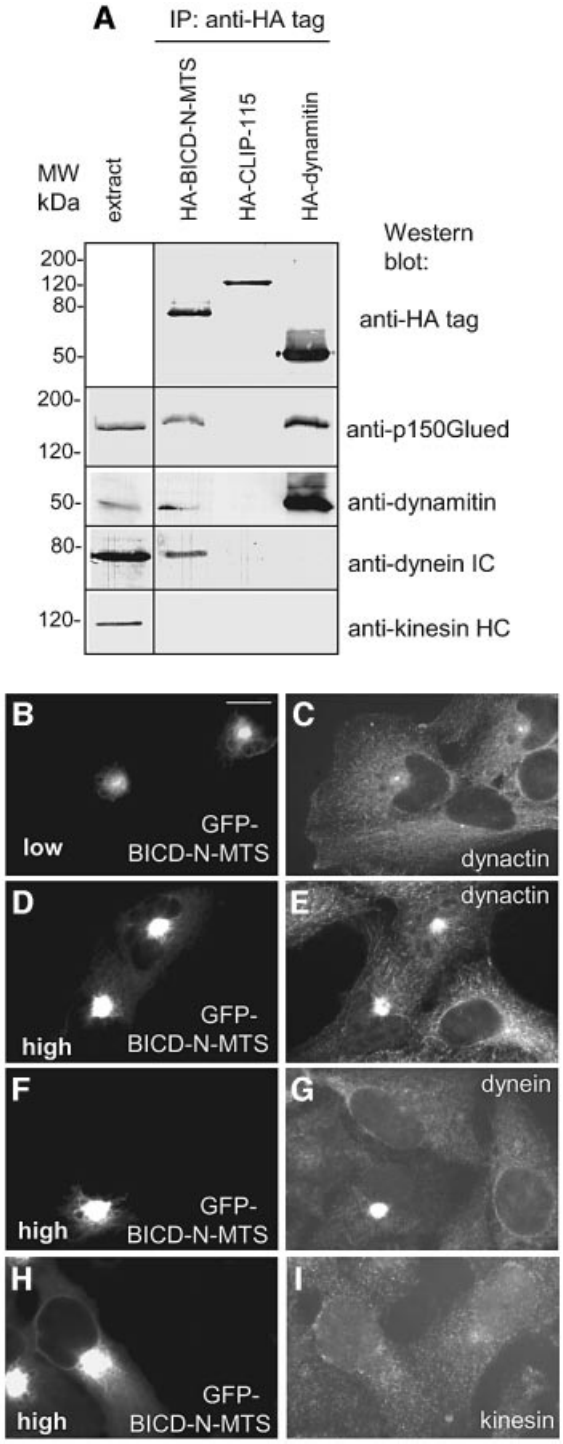

Fig. 5. BICD N–terminus recruits dynein and dynactin. (**A**) COS-1 cells were transfected with the indicated HA-fusion constructs and used for immunoprecipitation with anti-HA antibodies. Immunoprecipitates were analyzed by western blotting, using antibodies against HA, $p150^{Glued}$, dynamitin, dynein intermediate chain (DIC) and MAB1614 against kinesin heavy chain (KHC). Western blot analysis with anti-KHC SUK4 antibody produced a similar result (not shown). (**B–I**) HeLa cells were transfected with GFP–BICD-N–MTS (GFP signal shown in B, D, F and H) and stained for $p150^{Glued}$, DIC and KHC (antibody SUK4, MAB1614 produced a similar result; data not shown). Cells expressing low (B) or high levels (D, F and H) of GFP–BICD-N–MTS are shown. Bar, 10 μm.

BICD2 N–terminus relocalizes protein complexes to the MTOC

Cytoplasmic dynein transports not only membrane organelles, but also individual proteins and protein complexes. To test if the BICD2 N–terminal domain can target cytosolic proteins for dynein transport, we have examined carefully the distribution of HA–BICD-N–FRB and GFP–FKBP2 fusion proteins before and after addition of the dimerizer (Figure 4A–G). In addition to being diffusely present in the cytoplasm, HA–BICD-N–FRB displayed a small accumulation around the MTOC in ~20% of transfected cells (Figure 4B). Before the addition of the dimerizer, GFP–FKBP2 was diffusely distributed in the cytoplasm and the nucleus and never accumulated at the MTOC (Figure 4C). One hour after the dimerizer addition, a small aggregate of GFP–FKBP2 could be detected around the MTOC in ~20% of HA–BICD-N–FRB-coexpressing cells (Figure 4E–G; note that dimerizer addition results in exclusion of GFP–FKBP2 from the nucleus due to its association with the cytoplasmic HA–BICD-N–FRB). This observation can be regarded as evidence of microtubule minus end-directed transport of these proteins. For obvious reasons, this transport cannot be visualized directly. It can only be inferred from the presence of MTOC-localized protein accumulation, the formation of which depends on the aggregation of the transported proteins at the MTOC. Such protein aggregation may be influenced by many different (possibly stochastic) factors, which might explain why only ~20% of transfected cells contain an aggregate.

If this interpretation is correct, one would expect a more bulky protein fusion to produce larger aggregates in these conditions. To test this idea, we have attached the GFP–FKBP2 protein to the actin-binding domain (ABD) of α-actinin and transfected it together with HA–BICD-N–FRB into HeLa cells (Figure 4A and H–P). Before the addition of the dimerizer, GFP–FKBP2–ABD localized predominantly to the stress fibres (Figure 4I). One hour after the dimerizer addition, a large GFP–FKBP2–ABD and actin-containing aggregate, which always colocalized with the MTOC, was observed in ~40% of transfected cells (Figure 4K–P). Prolonged incubation with the dimerizer after this transfection appeared to be cytotoxic (the cells acquired a rounded-up appearance and seemed to lose their attachment to the substrate). Taken together, these experiments further support the versatility of BICD-N fusions for the induction of MTOC-directed relocalization of cellular structures and suggest that, in addition to membrane organelles, it can act on protein complexes.

BICD2 N–terminus binds to both dynactin and dynein, but not to conventional kinesin or kinesin II

Collapse of mitochondria into the perinuclear region was previously observed after blocking conventional kinesin by different methods (De Vos *et al*., 1998, 2000; Tanaka *et al*., 1998; Stowers *et al*., 2002). It should be noted that in kinesin inhibition experiments, mitochondria retained

their normal shape, and a dense aggregate was never formed. Therefore, we believe that the primary effect of targeting BICD-N domain to organelles is the recruitment of the dynein motor, rather than inhibition of kinesin. To obtain further support for this view, we performed immunoprecipitation experiments with HA- or GFP-tagged BICD-N–MTS fusions, using similarly tagged dynamitin and CLIP-115 proteins as controls. In line with our previous observations (Hoogenraad *et al*., 2001), a significant amount of dynein complex was co-precipitated with BICD-N–MTS, but not with the control constructs (Figure 5A). In addition we noticed, that, similar to dynamitin, BICD-N–MTS pulled down dynactin, while none of the three tested proteins was able to co-precipitate kinesin heavy chain (Figure 5A) or components of the heterotrimeric kinesin II complex KIF3A and KAP3A (data not shown). It seems unlikely that conventional kinesin or kinesin II interact directly with BICD proteins, since they were not precipitated with the endogenous full-length BICD1 and BICD2 proteins either (data no shown).

In agreement with immunoprecipitation experiments, both dynein and dynactin were concentrated in the region of the mitochondrial cluster in cells, expressing high levels of GFP–BICD-N–MTS (Figure 5D–G). In cells with low or medium expression levels of this fusion, dynein and dynactin were distributed normally (Figure 5B and C), indicating that dramatic relocalization of these complexes was not required for the aggregation of mitochondria and peroxisomes. Subcellular distribution of conventional kinesin and kinesin II (KIF3A and KAP3A) was not substantially affected by the expression of GFP–BICD-N–MTS (Figure 5H and I; data not shown).

Analysis of sensitivity of BICD2-induced organelle displacement to dynein-inhibiting agents

As expected, the formation of the mitochondrial cluster in GFP–BICD–N-MTS-transfected cells was microtubule-dependent, since microtubule-depolymerizing drug nocodazole caused its dispersion, similar to the nocodazole-induced scattering of the Golgi apparatus (Figure 6A–C). Fifteen to twenty minutes after nocodazole washout the morphology of the mitochondrial aggregate was restored, again similar to the restoration of the Golgi complex after the same treatment (data not shown).

Cytoplasmic dynein-mediated transport can be disrupted by overexpression of the dynactin subunit dynamitin (Echeverri *et al*., 1996; Burkhardt *et al*., 1997). To our surprise, the dense clusters of mitochondria and peroxisomes, induced by the BICD-N–MTS fusions, displayed very limited sensitivity to the excess of dynamitin. In 63% of double-transfected cells, the mitochondrial cluster appeared unaffected by dynamitin overexpression (Figure 6D–F and P), while in the remaining 37% of cells increased formation of extended mitochondrial tubules and partial dispersion of the aggregates could be seen (Figure 6G–I and P). The latter effect, which correlated with the appearance of abnormally shaped, multilobular nuclei (Figure 6I; Supplementary figure 4F), could be to some extent accounted for by the disruption of the microtubule network due to dynamitin overexpression (Quintyne *et al*., 1999; Supplementary figure 4). Normally shaped, dispersed mitochondria were never observed in these double transfections, even in cells with low levels of BICD-N–MTS and high levels of dynamitin. Overexpression of another dynein-blocking agent, the first coiled coil segment of the dynactin large subunit p150Glued (p150-CC1; Quintyne *et al*., 1999), had no visible effect on the BICDN–MTS-induced mitochondrial cluster (Figure 6J–L and P), although, similar to dynamitin, it did cause the dispersion of the Golgi complex. However, when p150-CC1 and dynamitin were co-expressed together with BICD-N–MTS, they did block mitochondrial aggregation in ~12% of triple transfected cells (Figure 6M–P), possibly because they could cooperatively compete with dynein/dynactin complex for binding to BICD-N.

To obtain further support for dynein involvement in the BICD-N-mediated effects, we have microinjected into GFP–BICD-N–MTS-expressing cells a function-blocking antibody against dynein intermediate chain (M74–2; Steffen *et al*., 1997). This treatment caused disintegration of the mitochondrial cluster in cells, expressing medium levels of the fusion protein and increased tubulation and motility of mitochondria in cells, expressing high levels of the fusion (Figure 6Q–T; Supplementary movie 4; data not shown). Interestingly, in line with previous observations (De Vos *et al*., 1998), we have noticed that mitochondrial aggregation was highly cytotoxic and resulted in a loss of cell motility in migrating cells, such as CAR fish fibroblasts (data not shown). Microinjection of the M74–2 antibody alleviated this effect and resulted in partial restoration of cell migration (data not shown).

In contrast to the results obtained with BICD-N–MTS fusion, dynamitin overexpression could efficiently block the coalescence of mitochondria and peroxisomes, caused by the full-length BICD2 (GFP–BICD2–MTS fusion) in ~35% of cotransfected cells (Figure 7). Such sensitivity to inhibition by dynamitin is likely to reflect an important physiological property of the full-length BICD protein.

Discussion

Our data demonstrate that tethering of the N–terminal domain of BICD2 to membrane organelles has a dramatic

Fig. 6. Effect of dynein-inhibiting agents on the mitochondrial aggregation, caused by the BICD-N–MTS fusion. (**A**–**C**) HeLa cells were transfected with GFP-BICD-N-MTS (A), stained with MitoTracker (B) and treated with 10 μM nocodazole 1 h before fixation. An enlarged portion of the overlay (GFP signal in green, mitochondria in red) is shown in (C). (**D**–**O**) HeLa cells were cotransfected with the indicated constructs, stained with MitoTracker, fixed and stained for HA-tag. Anti-HA staining is shown in the left panels, MitoTracker in the middle panels and GFP signal in the right panels. Bar, 10 μm. (**P**) Quantitative analysis of the transfection results, shown in (D–O). For each cotransfection, three independent experiments were performed, and 100 cells were counted for each experiment. Only cells which had a healthy, spread appearance and expressed medium levels (5–10 times compared with the endogenous BICD2 levels, as determined by counterstaining with anti-BICD2 antibodies), were scored. Percentage of transfected cells, displaying the indicated phenotype is shown; standard deviations are indicated. (**Q**–**T**) CAR fish fibroblast, transfected with GFP-BICD-N-MTS, was microinjected with M74–2 antibody against dynein intermediate chain. GFP signal before and at different time intervals after transfection is shown. Bar, 10 μm.

effect on their subcellular distribution. Mitochondria and peroxisomes, like many other cellular structures, can be transported by both plus and minus-end directed microtubule motors (Goldstein and Yang, 2000; Schrader *et al*., 2000; Stamer *et al*., 2002). The actual localization of organelles depends on the balance of forces, exerted by the opposite polarity motors, which might be the result of their competition ('tug of war') or coordinated regulation (see

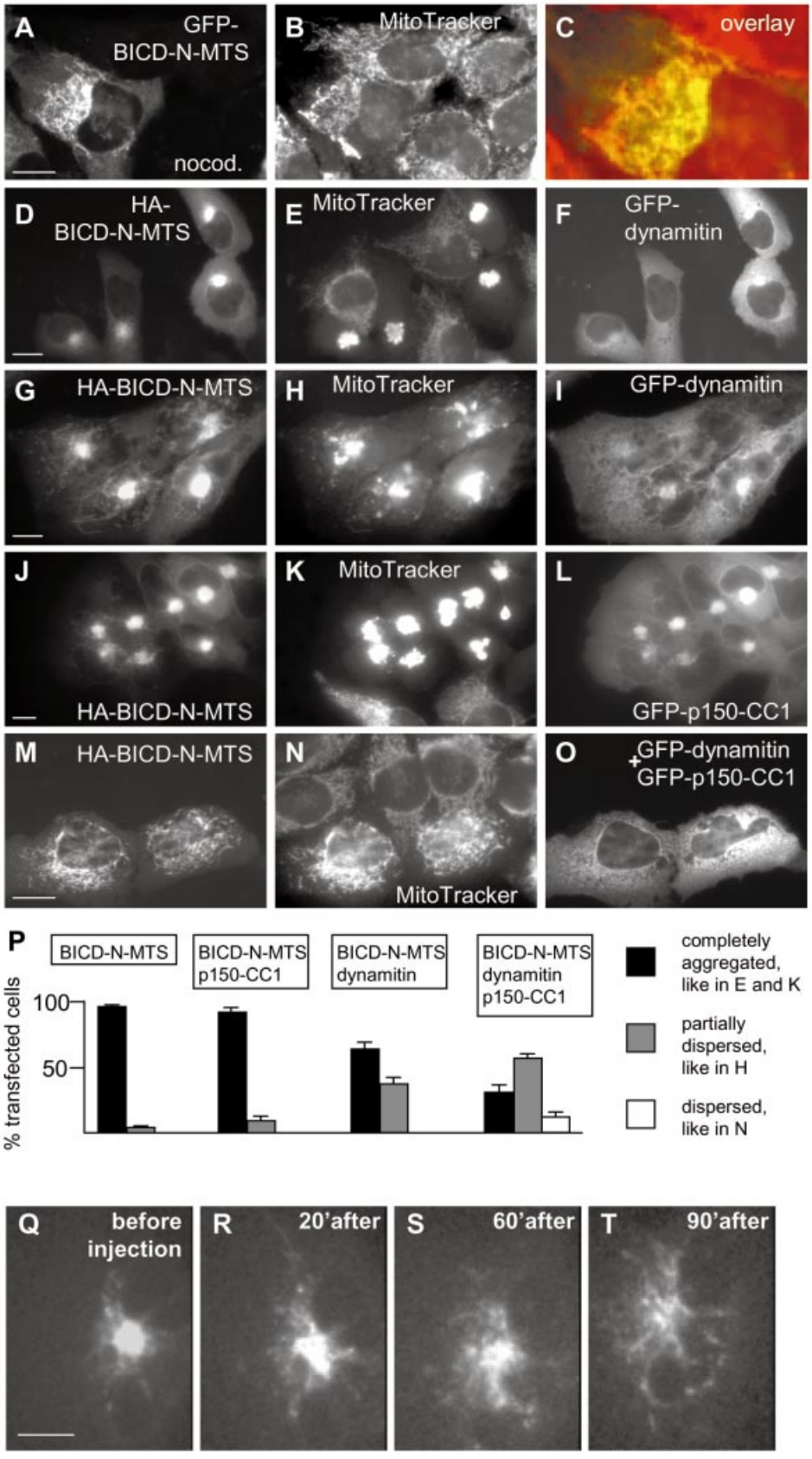

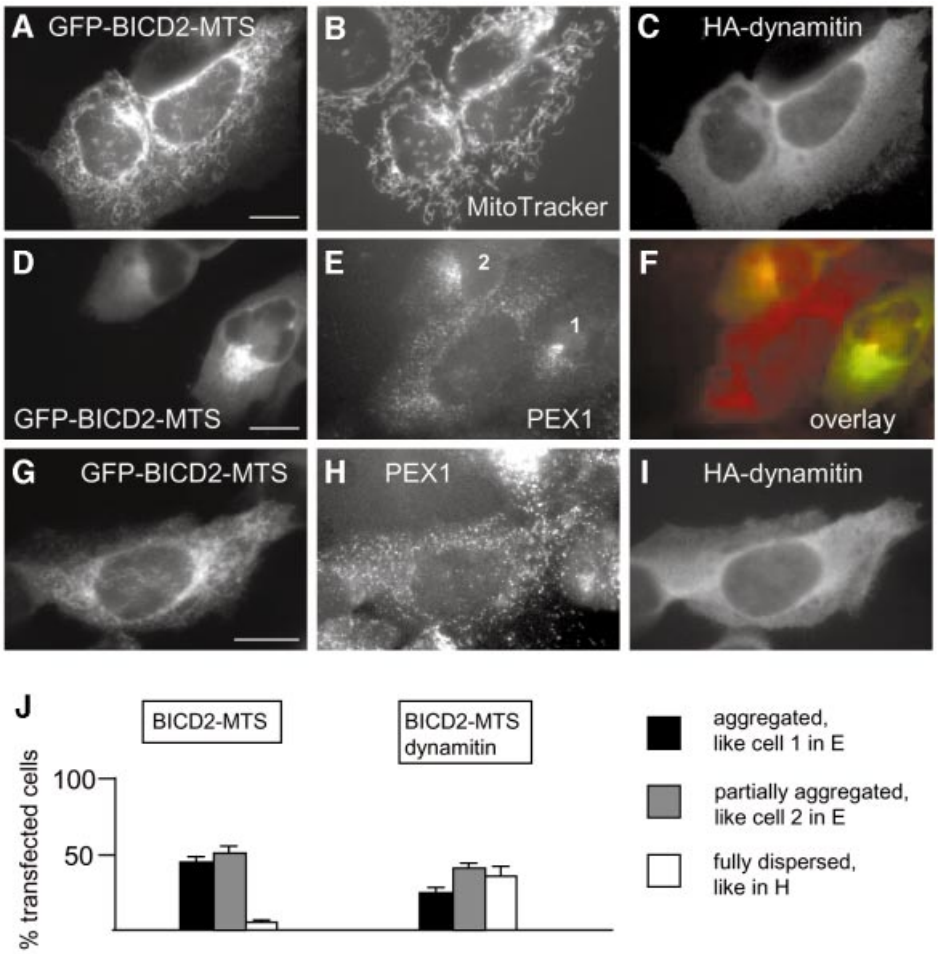

Fig. 7. Dynamitin inhibits aggregation of mitochondria and peroxisomes, caused by BICD2-MTS. (**A**–**C**) HeLa cells were cotransfected with GFP-BICD2-MTS and HA-dynamitin, stained with MitoTracker, fixed and stained for HA-tag. GFP signal is shown in (A), MitoTracker signal in (B) and HA-specific signal in (C). (**D**–**F**) HeLa cells were transfected with GFP-BICD2-MTS (D) and stained for peroxisomal marker PEX1 (E), overlay is shown in (F) (GFP signal in green, PEX1 signal in red). (**G**–**I**) HeLa cells were cotransfected with GFP-BICD2-MTS (G) and HA-dynamitin and stained for PEX1 (H) and HA-tag (I). Bar, 10 μm. (**J**) Quantitative analysis of the transfection results, shown in (D–I), performed as described for Figure 6P. Only cells which had a healthy, spread appearance and expressed medium levels (5–10 times compared with the endogenous BICD2 levels, as determined by counterstaining with anti-BICD2 antibodies), were scored. Staining for peroxisomes, rather than mitochondria, was used here for quantification, because it allows better assessment of the partially and fully dispersed phenotypes.

Deacon *et al*., 2003; Gross, 2003; and references therein). It is clear that BICD protein, being targeted to a particular structure, is able to shift the balance in favour of the minus end-directed transport. Our results, together with the previously published genetic data from *Drosophila* and biochemical data from mammalian cells, support the notion that cytoplasmic dynein is the motor responsible for this transport. Our observations clarify the role of the BICD protein and are in line with the model, in which the N–terminal domain of BICD acts as an anchor for dynein motor, while the C–terminal domain is responsible for cargo recognition.

We hypothesize that the N–terminal part of BICD protein makes contact with both dynein and dynactin and stabilizes the joint complex. This idea is in line with the observations that significant amounts of both complexes are co-precipitated with the BICD-N–MTS protein and that the transport, induced by BICD-N–MTS protein, is relatively insensitive to dynactin-derived inhibitory agents, such as dynamitin and p150-CC1. In our previous study we have not focussed on the binding partners of BICD2 N–terminal domain, because we could not find a direct interaction of this domain with dynactin components using the yeast two hybrid system (Hoogenraad *et al*., 2001). In addition, until now we were unable to identify the dynein components which make direct contact with the N–terminal part of BICD2 (C.Hoogenraad and A.Akhmanova, unpublished results). However, the recent data presented in this paper suggests that such interactions are likely to exist and may involve simultaneous binding to more than one dynactin component (for example $p150^{Glued}$ and dynamitin) or coordinated association with both dynein and dynactin components. It is likely that the conformation of dynein and dynactin subunits, when they are expressed individually, is different from their conformation within the native *in vivo* complex. This could be an explanation why we may have failed to detect a direct BICD-N–dynactin/dynein binding using separate dynein and dynactin subunits. It is interesting in this context that simultaneous overexpression of dynamitin and p150-CC1 significantly counteracted the BICD-N–MTS phenotype while the

individual components had limited effect. Further studies are necessary to investigate the direct binding partners of the BICD2 N–terminal domain.

Our previous results have shown that overexpression of the N–terminal BICD2 domain, when it is freely present in the cytoplasm, suppresses the dynein function (Hoogenraad *et al*., 2001). We have hypothesized that this might be due to formation of active dynein–dynactin complexes, which are not attached to cargo and cannot be recycled efficiently to transport other cargos. In this study we examined the distribution of BICD-N–FRB fusion proteins and found that they form an aggregate around the MTOC in a small percentage of transfected cells, suggesting that this protein might indeed undergo microtubule minus end-directed motility. Further, we show that BICD-N induces MTOC accumulation (presumably due to microtubule minus end-directed transport) of cargos, GFP–FKBP2 and GFP–FKBP2–ABD, which are generally not expected to be precomplexed with dynein and dynactin. It is noteworthy, that the aggregates, formed by GFP–FKBP2–ABD, were larger (probably because they also contained actin and possibly some other actin-associated cell components), than those formed by GFP–FKBP2 alone. This suggests that the possibility to detect minus end-directed transport in this way strongly depends on the capacity of the cargo to aggregate and not diffuse away from the MTOC. Together, these observations support the idea that BICD-N forms a complex with dynein and dynactin which is either active or can be activated easily and that BICD-N is able to recruit dynein to cargos which are normally not associated with it.

It has recently been shown that the dynactin $p150^{Glued}$ subunit interacts directly with kinesin II (Deacon *et al*., 2003; Gross, 2003). Therefore, dynactin might be switching between dynein and kinesin as binding partners, and this process could determine the direction of organelle movement. How such switching could occur remains unclear, but it is possible that proteins like BICD play a regulatory function, transiently stabilizing either dynactin–dynein or dynactin–kinesin complexes. Binding of BICD-N to the dynein–dynactin complex might cause an alteration in its conformation, which may be reflected in its incapacity to form aggregates, normally observed after nocodazole treatment (Hoogenraad *et al*., 2001).

We have shown that, compared with the N–terminal domain alone, the full-length BICD2 has a milder effect on organelle relocalization and is more sensitive to dynamitin-induced block of dynein transport. These data are in line with the suggestion that intramolecular interactions between BICD C- and N–terminal domains, and/or the previously identified interaction between BICD C–terminus and dynamitin have an attenuating effect on BICD-induced dynein motility. Therefore, in addition to cargo binding, the C–terminal coiled-coil domain of BICD appears to play a regulatory function, which is probably essential for the normal physiological role of the molecule, allowing the disengagement of the dynein motor.

The observation that the N–terminal domain of BICD2 is capable of inducing microtubule minus end-directed transport while placed in different molecular contexts could be exploited to efficiently relocalize different cellular components by using appropriate targeting motifs. In addition, the possibility to induce dynein-mediated transport of particular organelles, proteins or other intracellular constituents by adding a small cell permeable compound could provide a useful tool to study the molecular details of dynein motility.

Materials and methods

Construction of expression vectors

All BICD2 fusion constructs were generated from mouse BICD2 cDNA (Hoogenraad *et al*., 2001) in pEGFP-C vectors by PCR-based technology. MTS sequence was derived from the plasmid pSPL61 (Bubeck *et al*., 1997), a kind gift from S.Pistor. FRB and FKBP-encoding fragments were from Argent Regulated Heterodimerization kit (Ariad Pharmaceuticals, http://www.ariad.com/regulationkits). GFP–PEX3–GFP was a gift from B.Distel (Voorn-Brouwer *et al*., 2001). GFP–ABD, including amino acids 34–246 of the chicken α-actinin was a gift from M.Gimona. Human LIC2 (DDBJ/EMBL/GenBank accession number NM_006141) was obtained by RT–PCR using human brain cDNA as a template and verified by sequencing. Mouse IC2 (DDBJ/EMBL/GenBank accession number NM_010064) was obtained as an I.M.A.G.E. clone 3990138 from the ATCC and its coding region verified by sequencing. HA-tagged constructs were generated by substituting GFP for a triple HA tag in the corresponding GFP fusions. Rat $p150^{Glued}$ cDNA (a gift from Dr K.Vaughan) was used to generate GFP-p150-CC1 construct (encoding amino acids 208–546 of the $p150^{Glued}$ protein). GFP–dynamitin was a gift from Dr T.Schroer.

Cell culture, transfection, immunofluorescence analysis, immunoprecipitation and western blotting

HeLa or COS-1 cells were grown, transfected and processed for immunofluorescence or western blotting as described earlier (Hoogenraad *et al*., 2000, 2001). Mitochondria were visualized using MitoTracker Red CMXRos (Molecular probes) according to the manufacturer's instructions. Dimerization of FRB and FKBP-containing proteins was induced by addition of AP21967 (Ariad Pharmaceuticals), dissolved in ethanol, to a final concentration of 125 nM. Mouse monoclonal antibodies against $p150^{Glued}$, PEX1, GM130 (Transduction Laboratories), transferrin receptor and GFP (Roche), dynein intermediate chain (IC74, Chemicon), HA tag (clone 16B12; Babco), kinesin heavy chain MAB1614 (Chemicon) and SUK4 (Cytoskeleton) were diluted 1:100 for immunofluorescence and 1:1000 for western blotting. For western blotting, alkaline phosphatase-conjugated goat anti-mouse secondary antibodies (Sigma) were used in a dilution 1:2500. The secondary antibodies used in immunofluorescence experiments were Alexa 594-conjugated goat anti-mouse and Alexa-350-conjugated sheep anti-mouse (1:300, Molecular Probes). Slides were mounted using Vectashield mounting medium (Vector laboratories) and analyzed with a Leica DMRBE microscope, equipped with a Hamamatsu CCD camera (C4880).

To quantify the levels of expression of the fusion proteins, GFP–BICD2–MTS- and GFP–BICD-N–MTS-expressing cells were stained with the antibody 2293, directed against the N–terminal part of the BICD2 protein (see Supplementary figure 5 for an example of such staining). The epitopes, recognized by this antibody, are fully contained within the BICD-N fusions, used in this study. Fluorescence intensity measurements were performed using MetaMorph image analysis software (Universal Imaging Corporation). The level of overexpression in GFP–BICD-N–MTS-transfected cells was quantified by measuring the average immunofluorescence intensity of the BICD2 antibody 2293 in transfected and untransfected cells. To relate the levels of overexpression of transfected proteins to the endogenous BICD2 level, the ratio of average fluorescence intensity was obtained by comparing values of the BICD2 antibody 2293 staining in transfected versus untransfected cells in the same image. Cells with a ratio of 2–5, 5–10 and 10–25 were defined as low, medium and high expressing cells, respectively. In addition, direct GFP fluorescence was used to compare expression levels of GFP-fusions between the experiments where cells were stained with BICD2-specific antibodies or with other markers.

Immunoprecipitation experiments were performed using HeLa cells, transfected with Lipofectamine 2000 (Invitrogen) or COS-1 cells, transfected with DEAE–dextran method (Hoogenraad *et al*., 2000) as described before (Hoogenraad *et al*., 2001), using anti-GFP and anti-HA monoclonal antibodies in a dilution of 1:50.

Live cell imaging and microinjection

Glass coverslips with HeLa cells, transfected using SuperFect (Qiagen), were mounted in an Attofluor cell chamber (Molecular Probes). Cells were analyzed in a 37°C heating chamber, on a Zeiss 510 confocal laser scanning microscope (LSM510), with lens heating, as described previously (Matanis *et al*., 2002). Images were recorded and movies assembled using the software package of the LSM 510 (Z-stack in all cases was 1 μm).

Goldfish CAR fibroblasts (ATCC) were transfected using SuperFect. Cells were microinjected with the M-74–2 antibody (kindly donated by Dr W.Steffen) or Cy3-labelled tubulin (kindly provided by Dr F.Severin) as described previously (Krylyshkina *et al*., 2002). Fibroblasts were observed at room temperature on an inverted microscope (Axiovert 135 TV, Carl Zeiss) equipped for epifluorescence and phase-contrast microscopy, using a 100X/NA 1.4 Plan-Apochromat objective. Data were acquired with a back-illuminated, cooled CCD camera from Princeton Research Instruments driven by IPLabs software (both from Visitron Systems, Pucheim, Germany) and stored as 16-bit digital images.

Supplementary data

Supplementary data are available at *The EMBO Journal* Online.

Acknowledgements

We would like to thank Drs W.Steffen, S.Pistor, T.Schroer, K.Vaughan, F.Severin, M.Gimona and B.Distel for the gift of materials. This research was supported by grants from the Netherlands Organization for Scientific Research and the Erasmus University to A.A. and C.H.

References

Allan,V. (2000) Dynactin. *Curr. Biol.*, **10**, R432.

Baens,M. and Marynen,P. (1997) A human homologue (BICD1) of the *Drosophila* bicaudal-D gene. *Genomics*, **45**, 601–606.

Bear,J.E., Loureiro,J.J., Libova,I., Fassler,R., Wehland,J. and Gertler,F.B. (2000) Negative regulation of fibroblast motility by Ena/VASP proteins. *Cell*, **101**, 717–728.

Bubeck,P., Pistor,S., Wehland,J. and Jockusch,B.M. (1997) Ligand recruitment by vinculin domains in transfected cells. *J. Cell Sci.*, **110**, 1361–1371.

Bullock,S.L. and Ish-Horowicz,D. (2001) Conserved signals and machinery for RNA transport in *Drosophila* oogenesis and embryogenesis. *Nature*, **414**, 611–616.

Burkhardt,J.K., Echeverri,C.J., Nilsson,T. and Vallee,R.B. (1997) Overexpression of the dynamitin (p50) subunit of the dynactin complex disrupts dynein-dependent maintenance of membrane organelle distribution. *J. Cell Biol.*, **139**, 469–484.

De Vos,K., Goossens,V., Boone,E., Vercammen,D., Vancompernolle,K., Vandenabeele,P., Haegeman,G., Fiers,W. and Grooten,J. (1998) The 55-kDa tumor necrosis factor receptor induces clustering of mitochondria through its membrane-proximal region. *J. Biol. Chem.*, **273**, 9673–9680.

De Vos,K., Severin,F., Van Herreweghe,F., Vancompernolle,K., Goossens,V., Hyman,A. and Grooten,J. (2000) Tumor necrosis factor induces hyperphosphorylation of kinesin light chain and inhibits kinesin-mediated transport of mitochondria. *J. Cell Biol.*, **149**, 1207–1214.

Deacon,S.W., Serpinskaya,A.S., Vaughan,P.S., Lopez Fanarraga,M., Vernos,I., Vaughan,K.T. and Gelfand,V.I. (2003) Dynactin is required for bidirectional organelle transport. *J. Cell Biol.*, **160**, 297–301.

Echeverri,C.J., Paschal,B.M., Vaughan,K.T. and Vallee,R.B. (1996) Molecular characterization of the 50-kD subunit of dynactin reveals function for the complex in chromosome alignment and spindle organization during mitosis. *J. Cell Biol.*, **132**, 617–633.

Goldstein,L.S. and Yang,Z. (2000) Microtubule-based transport systems in neurons: the roles of kinesins and dyneins. *Annu. Rev. Neurosci.*, **23**, 39–71.

Gross,S.P. (2003) Dynactin: coordinating motors with opposite inclinations. *Curr. Biol.*, **13**, R320–R322.

Helfand,B.T., Mikami,A., Vallee,R.B. and Goldman,R.D. (2002) A requirement for cytoplasmic dynein and dynactin in intermediate filament network assembly and organization. *J. Cell Biol.*, **157**, 795–806.

Hirokawa,N., Noda,Y. and Okada,Y. (1998) Kinesin and dynein superfamily proteins in organelle transport and cell division. *Curr. Opin. Cell Biol.*, **10**, 60–73.

Hoogenraad,C.C., Akhmanova,A., Grosveld,F., De Zeeuw,C.I. and Galjart,N. (2000) Functional analysis of CLIP-115 and its binding to microtubules. *J. Cell Sci.*, **113**, 2285–2297.

Hoogenraad,C.C., Akhmanova,A., Howell,S.A., Dortland,B.R., De Zeeuw,C.I., Willemsen,R., Visser,P., Grosveld,F. and Galjart,N. (2001) Mammalian Golgi-associated Bicaudal-D2 functions in the dynein–dynactin pathway by interacting with these complexes. *EMBO J.*, **20**, 4041–4054.

Karki,S. and Holzbaur,E.L. (1999) Cytoplasmic dynein and dynactin in cell division and intracellular transport. *Curr. Opin. Cell Biol.*, **11**, 45–53.

King,S.J. and Schroer,T.A. (2000) Dynactin increases the processivity of the cytoplasmic dynein motor. *Nat. Cell Biol.*, **2**, 20–24.

Krylyshkina,O., Kaverina,I., Kranewitter,W., Steffen,W., Alonso,M.C., Cross,R.A. and Small,J.V. (2002) Modulation of substrate adhesion dynamics via microtubule targeting requires kinesin-1. *J. Cell Biol.*, **156**, 349–359.

Ligon,L.A., Karki,S., Tokito,M. and Holzbaur,E.L. (2001) Dynein binds to beta-catenin and may tether microtubules at adherens junctions. *Nat. Cell Biol.*, **3**, 913–917.

Matanis,T. *et al.* (2002) Bicaudal-D regulates COPI-independent Golgi–ER transport by recruiting the dynein–dynactin motor complex. *Nat. Cell Biol.*, **4**, 986–992.

Muresan,V., Stankewich,M.C., Steffen,W., Morrow,J.S., Holzbaur,E.L. and Schnapp,B.J. (2001) Dynactin-dependent, dynein-driven vesicle transport in the absence of membrane proteins: a role for spectrin and acidic phospholipids. *Mol. Cell*, **7**, 173–183.

Pistor,S., Chakraborty,T., Niebuhr,K., Domann,E. and Wehland,J. (1994) The ActA protein of *Listeria monocytogenes* acts as a nucleator inducing reorganization of the actin cytoskeleton. *EMBO J.*, **13**, 758–763.

Pollock,R., Issner,R., Zoller,K., Natesan,S., Rivera,V.M. and Clackson,T. (2000) Delivery of a stringent dimerizer-regulated gene expression system in a single retroviral vector. *Proc. Natl Acad. Sci. USA*, **97**, 13221–13226.

Purohit,A., Tynan,S.H., Vallee,R. and Doxsey,S.J. (1999) Direct interaction of pericentrin with cytoplasmic dynein light intermediate chain contributes to mitotic spindle organization. *J. Cell Biol.*, **147**, 481–492.

Quintyne,N.J., Gill,S.R., Eckley,D.M., Crego,C.L., Compton,D.A. and Schroer,T.A. (1999) Dynactin is required for microtubule anchoring at centrosomes. *J. Cell Biol.*, **147**, 321–334.

Rivera,V.M. *et al.* (1996) A humanized system for pharmacologic control of gene expression. *Nat. Med.*, **2**, 1028–1032.

Schnorrer,F., Bohmann,K. and Nusslein-Volhard,C. (2000) The molecular motor dynein is involved in targeting swallow and bicoid RNA to the anterior pole of *Drosophila* oocytes. *Nat. Cell Biol.*, **2**, 185–190.

Schrader,M., King,S.J., Stroh,T.A. and Schroer,T.A. (2000) Real time imaging reveals a peroxisomal reticulum in living cells. *J. Cell Sci.*, **113**, 3663–3671.

Schroer,T. (1996) Structure and function of dynactin. *Semin. Cell Dev. Biol.*, **7**, 321–328.

Short,B., Preisinger,C., Schaletzky,J., Kopajtich,R. and Barr,F.A. (2002) The Rab6 GTPase regulates recruitment of the dynactin complex to Golgi membranes. *Curr. Biol.*, **12**, 1792–1795.

Soukupova,M., Sprenger,C., Gorgas,K., Kunau,W.H. and Dodt,G. (1999) Identification and characterization of the human peroxin PEX3. *Eur. J. Cell Biol.*, **78**, 357–374.

Stamer,K., Vogel,R., Thies,E., Mandelkow,E. and Mandelkow,E.M. (2002) Tau blocks traffic of organelles, neurofilaments and APP vesicles in neurons and enhances oxidative stress. *J. Cell Biol.*, **156**, 1051–1063.

Steffen,W., Karki,S., Vaughan,K.T., Vallee,R.B., Holzbaur,E.L., Weiss,D.G. and Kuznetsov,S.A. (1997) The involvement of the intermediate chain of cytoplasmic dynein in binding the motor complex to membranous organelles of *Xenopus* oocytes. *Mol. Biol. Cell*, **8**, 2077–2088.

Stowers,R.S., Megeath,L.J., Gorska-Andrzejak,J., Meinertzhagen,I.A. and Schwarz,T.L. (2002) Axonal transport of mitochondria to synapses depends on milton, a novel *Drosophila* protein. *Neuron*, **36**, 1063–1077.

Suter,B., Romberg,L.M. and Steward,R. (1989) Bicaudal-D, a *Drosophila* gene involved in developmental asymmetry: localized

transcript accumulation in ovaries and sequence similarity to myosin heavy chain tail domains. *Genes Dev.*, **3**, 1957–1968.

Swan,A., Nguyen,T. and Suter,B. (1999) *Drosophila* Lissencephaly-1 functions with Bic-D and dynein in oocyte determination and nuclear positioning. *Nat. Cell Biol.*, **1**, 444–449.

Tai,A.W., Chuang,J.Z., Bode,C., Wolfrum,U. and Sung,C.H. (1999) Rhodopsin's carboxy-terminal cytoplasmic tail acts as a membrane receptor for cytoplasmic dynein by binding to the dynein light chain Tctex-1. *Cell*, **97**, 877–887.

Tanaka,Y., Kanai,Y., Okada,Y., Nonaka,S., Takeda,S., Harada,A. and Hirokawa,N. (1998) Targeted disruption of mouse conventional kinesin heavy chain, kif5B, results in abnormal perinuclear clustering of mitochondria. *Cell*, **93**, 1147–1158.

Voorn-Brouwer,T., Kragt,A., Tabak,H.F. and Distel,B. (2001) Peroxisomal membrane proteins are properly targeted to peroxisomes in the absence of COPI- and COPII-mediated vesicular transport. *J. Cell Sci.*, **114**, 2199–2204.

Wharton,R.P. and Struhl,G. (1989) Structure of the *Drosophila* BicaudalD protein and its role in localizing the the posterior determinant nanos. *Cell*, **59**, 881–892.

Received May 15, 2003; revised September 10, 2003;
accepted October 2, 2003